Volume 20 (2001), number 4 pp. 189–199 COMPUTER GRAPHICS *forum*

Rendering Natural Waters

Simon Premože and Michael Ashikhmin

Department of Computer Science, University of Utah, Salt Lake City, Utah, USA
premoze@cs.utah.edu, michael@cs.utah.edu

Abstract
Creating and rendering realistic water is one of the most daunting tasks in computer graphics. Realistic rendering of water requires that the sunlight and skylight illumination are correct, the water surface is modeled accurately and that the light transport within water body is properly handled. This paper describes a method for wave generation on a water surface using a physically-based approach. The wave generation uses data from the oceanographical observations and it is controlled by intuitive parameters such as wind speed and wind direction. The optical behavior of the water surfaces is complex but is well-described in the ocean science literature. We present a simple and intuitive light transport approach that is easy to use for many different water types such as deep ocean water, muddy coastal water, and fresh water bodies. We demonstrate our model for a number of water and atmospheric conditions.

Keywords: Rendering Realistic Water, Illumination, Optical Behavior

1. Introduction

Of all the challenges facing those who create computer-generated imagery, one of the most daunting is creating realistic water. To create realistic images of water three components need to be addressed:

(1) **Atmospheric conditions:** What direction and magnitude does the wind that generates waves have? How much sunlight and skylight reaches the water surface?
(2) **Wave generation:** What makes the water look like the ocean?
(3) **Light transport:** How does light interact with the water body?

In this paper we address the second and third points only. Our work differs from the previous work described below because we use a methodology customized to the real data available in the oceanographic literature.

Water has many components to its subjective appearance that must be accounted for in any realistic rendering. The water's reflectivity will vary between 5 and 100%, depending on angle. For angles where the reflectivity is high, the sky will be reflected with little loss of intensity. Where water's orientation reflects the disk of the sun, extremely bright highlights are present. The spatial pattern of such highlights are very familiar. Where the reflectivity of the water surface is low, any light coming from below the surface should be visible to the viewer. This light can be reflected light from the water bottom, or scattered light from the water volume itself. The impurities in the water determine the amount of scatter by the volume, as well as its color. Thus the familiar brown of muddy water and the deep blue of many tropical waters. To capture the appearance of water, this scattering must be approximated with sufficient accuracy to recreate these familiar opacities and colors. Minnaert describes many of these effects [1].

Perlin has used a noise synthesis approach [2] to simulate the appearance of the ocean surface seen from a distance. More in-depth discussion of water waves in computer graphics was presented by Fournier and Reeves [3], Peachey [4], and Ts'o and Barsky [5] who modeled shallow water waves using different basis shapes. Mastin *et al.* [6] described a technique long in use by the oceanography community for modeling deep ocean waves.

Figure 1: *Photograph of the ocean (left) and rendering (right) of ocean using technique described in the paper.*

Knowledge of the radiance distribution within and leaving a water body is a prerequisite for the solution of many problems in underwater visibility, remote sensing, mixed-layer thermodynamics, and realistic image synthesis. Watt describes a backward beam tracing approach to interaction of light with water [7], but his method does not take into account complex optical properties of water bodies. Nishita and Nakamae presented a method that can effectively calculate optical effects [8]. Their method focuses primarily on effects such as caustics and shafts of light in water bodies.

In this paper we describe an approach to modeling water surfaces based on simple atmospheric conditions and solving a light transport in water bodies that is simple and efficient, and yet accurate enough for many different water types ranging from deep ocean water to muddy coastal waters and freshwaters.

2. Wave Generation and Animation

The importance of plausible modeling of any water surface is two-fold. First, the visual characteristics of water surfaces especially oceans are very distinct. Second, it has been well known in oceanographic community that fluctuations in the marine light field are dominated by the variability of the air–sea interface [9].

In our model we assume that the surface waves are assembled from many linear waves generated by wind over an area much larger than the correlation length of the waves [10]. Therefore, the important water surface descriptors such as displacement and slope can be represented as normally distributed Gaussian random variables. Experimental measurements of surface-wave statistics confirm that these water surface descriptors have Gaussian distributions which are independent and statistically invariant. Mastin *et al.* [6] introduced this long-known surface wave synthesis method [11] to the computer graphics community. The procedure uses a sum of sinusoidal amplitudes and phases and is based on empirical observations of oceans. The height of the water surface at the location $\vec{\mathbf{x}}$ on the grid and time t is

$$\eta(\vec{\mathbf{x}}, t) = \sum_{\vec{\mathbf{k}}} \hat{\eta}(\vec{\mathbf{k}}, t)\, \mathrm{e}^{i\vec{\mathbf{k}}\vec{\mathbf{x}}}, \tag{1}$$

where $\vec{\mathbf{k}}$ is wave vector pointing in a direction of travel of the wave, and $\hat{\eta}(\vec{\mathbf{k}}, t)$ is the time-dependent Fourier component of the water surface:

$$\hat{\eta}(\vec{\mathbf{k}}, t) = \eta(\vec{\mathbf{k}})\, \mathrm{e}^{i\omega(k)t}. \tag{2}$$

The spatial spectrum $P_h(\vec{\mathbf{k}})$ is ensemble average

$$P_h(\vec{\mathbf{k}}) = \langle |\hat{\eta}(\vec{\mathbf{k}}, t)| \rangle. \tag{3}$$

Pierson and Moskowitz developed a model based on ship-recorded measurements describing height profile of a fully developed wind-driven sea [12]. The downwind *Pierson–Moskowitz* power spectrum is

$$F_{\mathrm{PM}}(f) = \frac{ag^2}{(2\pi)^4 f^5}\, \mathrm{e}^{-\frac{5}{4}\left(\frac{f_m}{f}\right)^4}, \tag{4}$$

where f is the frequency, a is the *Phillips* constant, g is the gravitational acceleration at sea level, and f_m is a peak frequency. f_m depends on the wind speed U_{10} that is measured 10 m above the sea surface:

$$f_m = \frac{0.13g}{U_{10}}. \tag{5}$$

The Pierson–Moskowitz spectrum assumes a fully developed sea in which the spectrum no longer grows given a constant wind velocity. Another approximation is that the influence of the sea floor on wave directions and amplitudes is not included. This means that the shoreline effects, such as the increase of wave amplitude on shallow water will not be handled. A more sophisticated model is required to treat these effects properly. Our model employs the *JONSWAP* two-dimensional power spectrum [13], where a directional spreading factor based on a wind direction $\vec{\mathbf{u}}$ is also taken into account:

$$F_{\mathrm{J}}(f, \theta) = F_{\mathrm{PM}} D(f, \theta), \tag{6}$$

where angle θ is measured with respect to wind direction $\vec{\mathbf{u}}$. Directional spreading is expressed as

$$D(f, \theta) = \frac{1}{N_{\mathrm{p}}} \cos^{2p}\left(\frac{\theta}{2}\right), \tag{7}$$

where

$$p = 9.77\left(\frac{f}{f_m}\right)^{\mu}$$

$$\mu = \begin{cases} 4.06 & \text{if } f < f_m \\ -2.34 & \text{otherwise} \end{cases}$$

$$N_{\mathrm{p}} = \frac{2^{1-2p}\pi\Gamma(2p+1)}{\Gamma^2(p+1)}$$

and Γ is the gamma function.

To obtain an ocean wave height field at particular time t, a white noise image seeded with a Gaussian random number generator is filtered with the JONSWAP spectrum from equation (6). This filtered white noise image is then transformed to spatial domain by an inverse Fourier transform. Other random number distributions can be used to model different waves. For example, Weibull or log-normal normal distributions could produce very flat waves [14]. The advantages of using the JONSWAP spectrum include the simplicity of its use and the ability to fine-tune the model. More traditional $\cos^2\theta$ directional spreading factors have broader profiles near the peak frequency in the downwind direction of the spectrum. Also, with traditional approaches, the peak frequency is not attenuated, thus allowing long-crested peak frequency components to run parallel to the wind direction. The only necessary parameter to our model is wind velocity. Although simple, it also enables an advanced user to fine tune the model as some of the parameters (invisible to most users) can be fit to measured and observed data for both oceans and lakes. Some of the more advanced parameters are available in [9] and [15].

So far we have only described how to compute the wave height field at one instant in time. To animate waves in a consistent manner we need to manipulate the phase of the waves. The dispersion relation for $\omega(k)$ states that the relationship between the magnitude of the wave vector $\vec{\mathbf{k}}$ and frequencies is

$$\omega^2(k) = gk. \tag{8}$$

The new time dependent Fourier amplitude is now computed using equation (2) with $\eta(\vec{\mathbf{k}})$ being the filtered spectrum as discussed earlier.

2.1. Whitecaps and foam

The wave generation model described thus far has omitted the effect of whitecaps and foam, which are present at wind speeds greater than a few meters per second. *Whitecaps* are the foamy part of actively breaking waves. The total foam area depends on the temperature difference between the air and the water and on water chemistry. The proper treatment of foam and whitecaps is very difficult [16], but some crude approximations can be made. Let f be the fractional area of the wind-blown water surface that is covered by foam. Monahan presents the following empirical formula [16]:

$$f = 1.59 * 10^{-5} U^{2.55} \exp[0.0861(T_{\mathrm{w}} - T_{\mathrm{a}})], \tag{9}$$

where U is wind speed, and T_{w} and T_{a} are the water and air temperatures in degrees Celsius. We use equation (9) to determine the fraction of water covered by foam that modifies optical properties on the water's surface. The reflectance of the ocean whitecap is therefore

$$\rho_{\mathrm{wc}}(\lambda) = f * \rho_{\mathrm{foam}}(\lambda) \tag{10}$$

where λ is wavelength of light and ρ_{foam} is the reflectance of pure foam (we use a Lambertian white reflectance as an approximation). However, the area of an individual whitecap increases with its age while the reflectance decreases. The fractional coverage f takes into account whitecaps of different ages and the whitecaps reflectance in equation (10) is too high. Koepke [17] provides a different formulation based on the empirical studies

$$\rho_{\mathrm{wc}}(\lambda) = f * f_{\mathrm{ef}} \rho_{\mathrm{foam}}(\lambda) \tag{11}$$

where f_{ef} is the efficiency factor ($f_{\mathrm{ef}} \approx 0.4 \pm 0.2$). As a crude approximation to the true distribution, one can put whitecaps at positions on the surface where the amplitude of the waves is the largest.

3. Light Transport

To generate realistic images of natural waters one must consider in some detail the interaction of light with the water body. In this section we will split this process into two major parts: events on the surface and light transport inside the water volume. Throughout the discussion we will assume that the viewpoint lies above the surface. This is done only for convenience (for example, we do not need to explicitly take into account n^2 law for radiance) and all the results with minor modifications are applicable to the more general case.

3.1. Across the surface

We treat water surface as a collection of locally planar facets and deal with light transport across a flat surface in a standard way. If a ray strikes part of the surface free from foam, it is split into reflected and transmitted (refracted) rays. Direction of the refracted ray is given by Snell's law $n_{\mathrm{i}} \sin\theta_{\mathrm{i}} = n_{\mathrm{t}} \sin\theta_{\mathrm{t}}$ where θ_{i} and θ_{t} are angles with the facet normal for incident and transmitted rays, respectively and n_{i}, n_{t} are real indices of refraction for the corresponding media. We set $n = 1$ and $n = 4/3$ for air and water respectively and ignore the slight dependence of these quantities on the wavelength of light. Snell's law shows that for a sufficiently oblique ray going from water to air it is possible to have total internal reflection when only reflected ray is present. This effect has to be checked for explicitly by the rendering software.

Reflectance and transmittance coefficients can be found from Fresnel formulae. Our rendering system uses full Fresnel expressions which can be found in any standard optics text, but a highly efficient and accurate approximation by Schlick is also available [18].

3.2. Within the water

Once photons from the sun and the sky pass through the air–water surface, they initiate a complex chain of scattering and absorption events within the water body. The behavior of radiance within natural water bodies is governed by the *radiance transfer equation*, a complex integro-differential equation which expresses changes in radiance along a path inside a water volume through the radiance itself and a number of water optical parameters. The task of finding radiance at a given point inside water body is therefore a prime example of the well known participating media problem, one of the hardest problems in computer graphics. A brute force approach to solving this problem for a large water volume would require an enormous amount of computation. Perhaps even more discouraging is the fact that values of optical parameters of natural waters are not easily obtainable with the precision needed for these computations. It is hard to justify computation of the final answer with high accuracy if the input data have an error of 10 or 20% which is not unusual for the type of data we need. Furthermore, optical properties of natural waters vary dramatically from open ocean to coastal waters to turbid harbor and even if accurate data are available for some conditions, they will be of no use in a different setting.

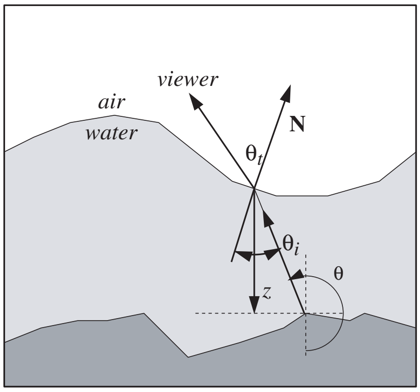

Figure 2: *Geometry of light transport. The propagation angle θ is counted from vertical "down" direction and for the geometry shown exceeds* 180°.

All this suggests an approach to the light transport problem which we briefly present now. We can not go into the details of marine optics which are needed to justify the simplification we made or derive some of the equations we use, for example, equations (16) or (17). We believe that the physical meaning of our equations should be clear for most readers familiar with the basics of light transport in a media. Those interested in a more formal presentation of the subject are referred to two classic texts [19,20]. If extreme detail is desired, the six volume treatise of Preisendorfer [21] is ideal. The sheer volume of the Preisendorfer's volumes testify to the complexity of the subject.

First, we simplify the problem by assuming the existence of two separate but related underwater light fields: the diffuse field radiance L_{df} due to combined effect of light scattered throughout the media and the directional radiance L which behavior we are ultimately interested in for rendering — this is what is being computed, for example, by a raytracer. L will contain a contribution due the diffuse field L_{df} and the other way around, so the two fields are not completely independent.

Second, we assume a uniform water body so that all optical properties are constant throughout. This approximation will manifest itself in our equations when we ignore the depth dependence of all water optical parameters. This will allow analytic integration of simplified light transport equations. Of course, if the effects due to inhomogeneity of water body are important, one would have to peform integration along each ray during rendering which would increase the runtime dramatically. We will also adopt the standard marine optics system of notation on Figure 2 with positive z-axis pointing down and angle θ to the propagating ray counted from this direction. Other important terms used in this section are summarized in Table 1.

Table 1: *Important terms used in the paper*

K_d	Diffuse attenuation coefficient for E_d
$K(\theta, \phi)$	Diffuse attenuation coefficient
E_d	Downwelling irradiance
E_u	Upwelling irradiance
R	Total path length
c	Beam attenuation coefficient
z	Water depth
L_*	In-scattered radiance
a	Absorption coefficient
b	Total scattering coefficient
b_b	Backscattering coefficient
t	Water turbidity
$L(\text{sky})$	Sky radiance
$L(\text{sun})$	Sun radiance

The change with depth of the diffuse radiance L_{df} propagating in direction (θ, ϕ) is given by

$$\frac{dL_{df}(z, \theta, \phi)}{dr} = -K(\theta, \phi)L_{df}(z, \theta, \phi)\cos\theta \quad (12)$$

where $K(\theta, \phi)$ is the *diffuse attenuation coefficient for radiance* in a given direction, z is the depth and $dr = -dz/\cos\theta$ is the differential path length which is always positive. This equation is the definition of the diffuse attenuation coefficient and comes directly from experimental observations. By simple integration we can write L_{df} dependence on depth as

$$L_{df}(z, \theta, \phi) = L_{df}(0, \theta, \phi)\, e^{K(\theta,\phi)z}. \quad (13)$$

Experimental evidence suggests that $K(\theta, \phi)$ is often independent of direction and moreover, its numerical value is very close to another coefficient which is much easier measured and for which numerical values, as a consequence, are much more readily available. This quantity is K_d, the *diffuse attenuation coefficient for downwelling irradiance* which definition also comes from the experimental relation:

$$K_d(z) = -\frac{d[\ln E_d(z)]}{dz} \quad (14)$$

where downwelling irradiance $E_d = \int_{\Omega_{down}} L\cos\theta d\Omega$ is introduced. E_d is easy to obtain since this is just a measure of the total energy propagating downwards and a measurement can be taken by a simple nondirectional sensor looking up. $K_d(z)$ is a slowly varying function of depth and its value K_d just beneath the surface is most commonly used. Complimentary to E_d quantity $E_u = \int_{\Omega_{up}} L\cos\theta d\Omega$ is called upwelling irradiance and can be similarly obtained. If both E_d and E_u are available, we can define *irradiance ratio S* as $S = E_u/E_d$. In a large number of experiments it was established that irradiance ratio is to the great accuracy a characteristic of water itself and does not depend on either E_u or E_d. A widely used relation expresses S through water optical parameters:

$$S \approx \frac{0.33b_b}{a} \quad (15)$$

where b_b is the backscattering coefficient and a is the absorption coefficient. We will use this equation below.

An alternative way to write the change in radiance is obtained if we note that it is due to two separate physical effects: losses from attenuation and gain from in-scattering:

$$\frac{dL_{df}(z, \theta, \phi)}{dr} = -cL_{df}(z, \theta, \phi) + L_*(z, \theta, \phi) \quad (16)$$

where c is *beam attenuation coefficient* and L_* is in-scattered radiance. Analogous equation holds for directional radiance:

$$\frac{dL(z, \theta, \phi)}{dr} = -cL(z, \theta, \phi) + L_*(z, \theta, \phi). \quad (17)$$

We will now integrate our light transport equations to derive apparent radiance just below the air–water interface $L(0)$ of the target at depth Z having its own radiance $L(Z)$. We will now introduce $R = -Z/\cos\theta$ which is the total path length for the ray from the target to the water surface and integrate our equations along this path. The last two equations suggest the following form for diffuse and directional radiances:

$$L_{df}(0, \theta, \phi) = L_{df}(Z, \theta, \phi)\, e^{-cR} + L_*^{tot}(Z, \theta, \phi) \quad (18)$$

$$L(0, \theta, \phi) = L(Z, \theta, \phi)\, e^{-cR} + L_*^{tot}(Z, \theta, \phi) \quad (19)$$

where L_*^{tot} is the total in-scattered radiance for the complete path. This quantity is the same in both equations and we can exclude it to obtain

$$L(0, \theta, \phi) = L(Z, \theta, \phi)\, e^{-cR} + L_{df}(0, \theta, \phi) - L_{df}(Z, \theta, \phi)\, e^{-cR}. \quad (20)$$

Finally, we can use equation (13) to obtain, after rearranging terms:

$$L(0, \theta, \phi) = L(Z, \theta, \phi)\, e^{-cR} + L_{df}(0)(1 - e^{(-c+K_d\cos\theta)R}). \quad (21)$$

This is the expression which we use during rendering. Here $L_{df}(0)$ is the diffuse radiance just below the sea surface which we will estimate below. This equation is a special case of a more general expression relating radiances at two arbitrary depths which can be obtained through the same procedure using different initial conditions in integration. Also note that according to our convention $\cos\theta$ is negative (for the viewing conditions shown on Figure 2) while all other values in equation (21) are positive. To estimate $L_{df}(0)$ we assume that radiance going upwards consists only of uniform diffuse light and use relation (15) between upwelling and downwelling irradiances:

$$L_{\mathrm{df}}(0) = \frac{E_{\mathrm{u}}(0)}{\pi} = \frac{SE_{\mathrm{d}}(0)}{\pi} \approx \frac{0.33 b_{\mathrm{b}}}{a}\left(\frac{E_{\mathrm{d}}(0)}{\pi}\right). \quad (22)$$

$E_{\mathrm{d}}(0)$ is the downwelling irradiance just below the surface which can be approximated as a sum of sun and sky contributions: $E_{\mathrm{d}}(0) = \pi L(\mathrm{sky}) + L(\mathrm{sun})\cos\theta_{\mathrm{sun}}$. We now have everything we need to perform light transport calculations once we know parameters b_{b}, a, c and K_{d}.

3.3. Optical parameter estimation

For a general case, all four optical parameters we need are independent from each other and we have to find measured or computed values for all of them separately. Moreover, to get the color of water right, we need the four optical parameters to vary with wavelength. Although theoretical models for these parameters do exist, they are quite complicated and, in turn, rely on even less readily available characteristics, such as scattering functions, phytoplankton concentrations, etc. Fortunately, a much simpler classification of natural waters exists. Jerlov [19] suggested a classification based on coefficient $K_{\mathrm{d}}(\lambda)$, experimental measurements of which over the entire visible spectrum for a given water type are available from many sources, for example [19,20] and [22]. He introduced twelve water types and assigned a particular $K_{\mathrm{d}}(\lambda)$ spectrum to each of them. Jerlov water types I to III are for open ocean waters with type I water being the clearest and type III being the most turbid. Types 1–9 correspond to coastal waters, again in progression from the clearest (type 1) to the most turbid (type 9).

These spectra are the only fully wavelength dependent input data required by our model. We will also use single wavelength values for the total scattering coefficient b provided for a given water type in [20] or [23].

Although naturally clear, water may look cloudy or muddy due to particles of matter suspended in it. This cloudy appearance is called *turbidity*. Turbidity affects the penetration of sunlight into a body of water. Algae and suspended particles of silt, plant fibers, sawdust, chemicals, and microorganisms are some of the causes of turbidity in water. We now introduce a single cumulative turbidity parameter t which assumes intuitive values in the interval from zero for clearest open ocean waters to one for very turbid harbor conditions. This parameter is used to obtain spectral data $K_{\mathrm{d}}(\lambda)$ and single number for b by interpolation of the input data. We then use simple approximate relations among water optical parameters presented below to obtain all the other coefficients. Much more accurate (and complicated) relations are available from the literature, but the simplest versions suffice for our purposes.

Table 2: *Diffuse attenuation coefficient for downwelling irradiance, $K_{\mathrm{d}}(\lambda)$, for different water types, in* $10^{-2}\mathrm{m}^{-1}$*, from* [19]

λ	Water type							
(nm)	I	II	III	1	3	5	7	9
310	15	37	65	180	240	350		
350	6.2	17.5	32	120	170	230	300	390
375	3.8	12.2	22	80	110	160	210	300
400	2.8	9.6	18.5	51	78	110	160	240
425	2.2	8.1	16	36	54	78	120	190
450	1.9	6.8	13.5	25	39	56	89	160
475	1.8	6.2	11.6	17	29	43	71	123
500	2.7	7.0	11.5	14	22	36	58	99
525	4.3	7.6	11.6	13	20	31	49	78
550	6.3	8.9	12.0	12	19	30	46	63
575	8.9	11.5	14.8	15	21	33	46	58
600	24	26	29.5	30	33	40	48	60
625	31	33.5	37.5	37	40	48	54	65
650	36	40	44.5	45	46	54	63	76
675	42	46.5	52	51	56	65	78	92
700	56	61	66	65	71	80	92	110

Table 3: *Total scattering coefficient b at* $\lambda_0 = 514$ nm *for different water types, from* [20]

Water type	$b(\mathrm{m}^{-1})$
Clear ocean (type I)	0.037
Coastal ocean (type 1)	0.219
Turbid harbor (type 9)	1.824

First of all, we obtain $a(\lambda) \approx K_{\mathrm{d}}$ [24]. Second, from the single $b(\lambda_0)$ we get $b(\lambda)$ and then $b_{\mathrm{b}}(\lambda)$ using very recently established [25] experimental relations

$$b(\lambda) = b(\lambda_0)\frac{m\lambda + i}{m\lambda_0 + i} \quad (23)$$

where $m = -0.001\,13$, $i = 1.625\,17$ and $b_{\mathrm{b}}(\lambda) = 0.018\,29 b(\lambda) + 0.000\,06$ and wavelength is expressed in nanometers. Finally, we use the definition $c(\lambda) = a(\lambda) + b(\lambda)$.

Our use of the turbidity parameter t is similar in spirit to that of Preetham *et al.* [26]. To make our model ready for immediate implementation, we provide wavelength-dependent values of K_{d} in Table 2 and values of b at $\lambda_0 = 514$ nm in Table 3. The data are from references [19] and [20], respectively. Exact assignment of the values of b to particular water type is somewhat arbitrary due to the absence of detailed data, but it should not make much visual difference.

Figure 3: *Shallow water in the tropics.*

In many cases phytoplankton and other particulate and dissolved material play a predominant role in determining the optical properies and color of water. If data or accurate measurements of particles dissolved in water are available we can also use concentration of this matter to determine scattering coefficients. Morel intoduced the following relation for the backscattering coefficient b_b [27]:

$$b_b(\lambda) = 0.5 b_w(\lambda) + B_b(\lambda) b_p \tag{24}$$

where $b_w(\lambda)$ is the molecular scattering coefficient of water, $B_b(\lambda)$ is the ratio of backscattering and scattering coefficients of the pigments and b_p is the scattering coefficient of the pigment. $B_b(\lambda)$ and $b_p(\lambda)$ are related to pigment concentration C (concentration of Chlorophyll A and Phtytoplankton in mg/m^3):

$$B_b(\lambda) = 0.002 + 0.02(0.5 - 0.25 \log_{10} C)\frac{550}{\lambda} \tag{25}$$

$$b_p(\lambda) = 0.3 C^{0.62}. \tag{26}$$

Table 4 shows typical concentration of chlorophyll and phytoplankton for some Jerlov water types. Note that the data are available only for open ocean water and care should be taken in using these numbers for coastal waters. This, once again, shows the benefits of our simple approach to optical parameter estimation which we presented in this section.

Table 4: *Approximate pigment concentration C for different open ocean water types* (*after Morel* [27])

Water type	C, $\frac{\text{mg}}{\text{m}^3}$
I	0.0–0.1
II	0.5
III	1.5–2

4. Present Results and Future Work

We have presented a method for wave generation and light transport in natural waters. The method uses a few simple and physically meaningful parameters that control both wave generation as well as the appearance of water bodies. Figure 6 shows renderings produced for oceans with different water types (deep water, muddy coastal water and tropical water). Figure 3 shows how the color of the water

Figure 4: *Different atmospheric conditions and whitecaps.*

Figure 5: *Island at sunset.*

changes with depth. Effects like this can often be observed in lakes and tropical islands. Figure 5 demonstrates that in order to make realistic images of water atmospheric conditions and illumination has to be computed accurately in addition to proper handling of wave generation and light transport in the water body. Figure 4 shows the same scene with different atmospheric conditions. Whitecaps can be seen during the stormy and rainy conditions. Figure 7 shows freshwater lake Crater Lake — a lake in volcanic caldera.

The water surface mesh and water type was input to a Monte Carlo path tracer [28] with a sky model similar to that used by Preetham *et al.* [26] that appropriately controls illumination based on time/date/place. For some of the images, sky environments were created using photographs [29] that were converted to high dynamic range environment maps and terrain rendering program Terragen [30] in which 360 degree sky panoramas were created. These sky maps were mapped onto a sky dome to increase visual richness of the sky but are not used to illuminate the scene. Glare effects were added in a post-processing step using a technique similar to [31].

We have also experimented with a more interactive approach which involves computation of the suffincluding height field using parallel FFT code and rendering the result with

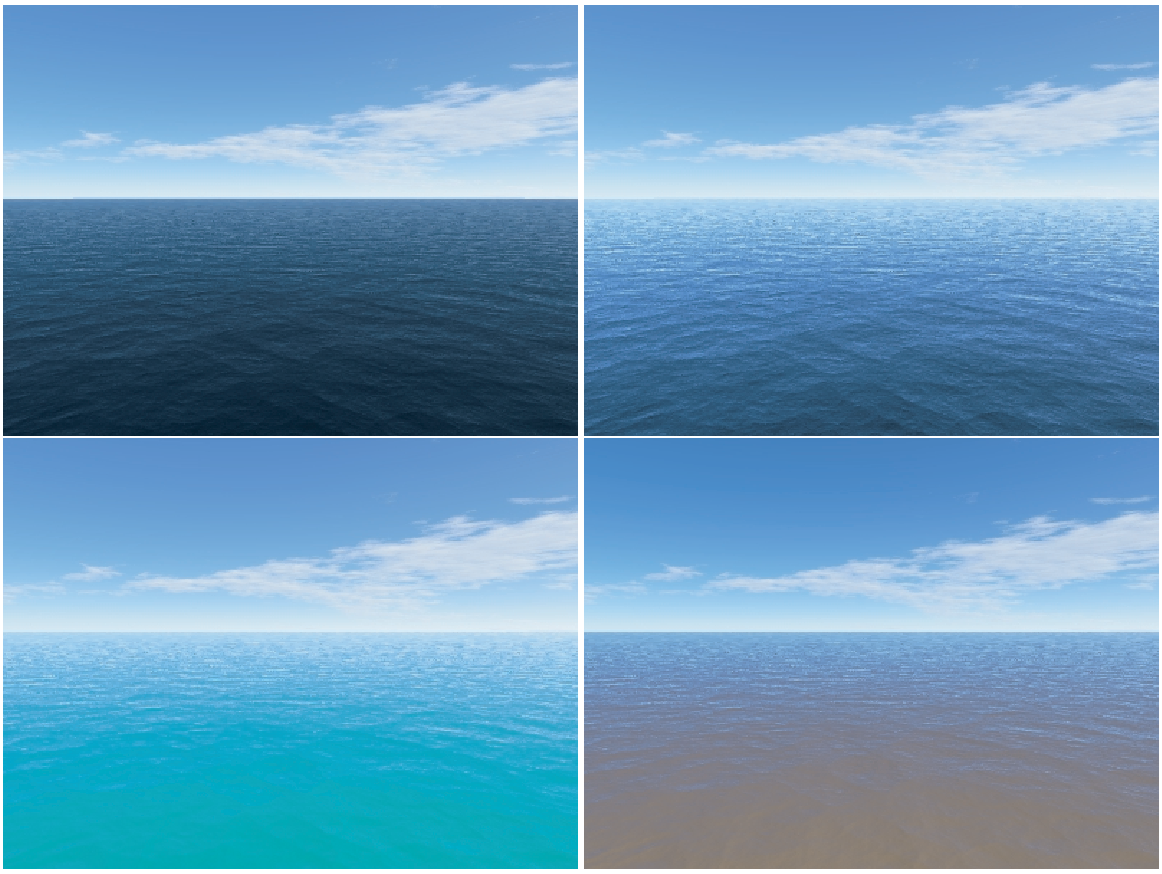

Figure 6: *Different water types: open ocean deep water (first row), tropical water (lower left), and muddy coastal water (lower right).*

Figure 7: *Crater Lake–freshwater lake in Oregon.*

the standard graphics hardware. With a 512×512 grid, which corresponds to a good quality height field (smallest wave feature of about 10 cm), we can obtain a frame rate of about two frames per second on a four processor SGI Onyx with 512 Mb of RAM and 2 Infinite Reality graphics pipes. For these experiments we concentrated on rendering water surface and did not include effects which are difficult in hardware (specularities, water depth effects, etc.).

Although this work showed some promising results there are many improvements needed to render and animate water. Breaking waves, wakes, and splashing cannot be rendered with the described method. Whitecaps and foam are not very well integrated into the wave generation. Furthermore, underwater sunbeams cannot be rendered due to the global nature of the effect. On the other hand, the method can easily be extended to accommodate caustics on underwater surfaces with some preprocessing and caustic image generation. Although the water waves can be animated, there are several difficulties when animation is concerned. Water has drastically different behavior at different scales. Water does not scale well because surface tension has different characteristics depending on scale. Animating objects in water and getting realistic motion is an extremely difficult task. Complex fluid dynamics is presently beyond realistic use due to the complexity of the phenomena and prohibitive computational costs.

References

1. M. Minnaert. *Light and Color in the Outdoors*. Springer, New York, 1974.
2. K. Perlin. An image synthesizer. In B. A. Barsky (ed), *Computer Graphics (SIGGRAPH '85 Proceedings)*. volume 19, pages 287–296. July 1985.
3. A. Fournier and W. T. Reeves. A simple model of ocean waves. In D. C. Evans and R. J. Athay (eds), *Computer Graphics (SIGGRAPH '86 Proceedings)*. volume 20, pages 75–84. August 1986.
4. D. R. Peachey. Modeling waves and surf. In D. C. Evans and R. J. Athay (eds), *Computer Graphics (SIGGRAPH '86 Proceedings)*. volume 20, pages 65–74. August 1986.
5. P. Y. Ts'o and B. A. Barsky. Modeling and rendering waves: wave-tracing using beta-splines and reflective and refractive texture mapping. *ACM Transactions on Graphics*, 6(3):191–214, 1987.
6. G. A. Mastin, P. A. Watterberg and J. F. Mareda. Fourier synthesis of ocean scenes. *IEEE Computer Graphics and Applications*, 16–23, March 1987.
7. M. Watt. Light–water interaction using backward beam tracing. In F. Baskett (ed), *Computer Graphics (SIGGRAPH '90 Proceedings)*. volume 24, pages 377–385. August 1990.
8. T. Nishita and E. Nakamae. Method of displaying optical effects within water using accumulation buffer. In A. Glassner (ed), *Proceedings of SIGGRAPH '94*. Pages 373–381. ACM Press, July 1994.
9. R. E. Walker. *Marine Light Field Statistics*. Wiley, New York, 1994.
10. O. M. Phillips. *The Dynamics of the Upper Ocean*. Cambridge University Press, Cambridge, 1977.
11. O. M. Phillips. On the generation of waves by turbulent wind. *Journal of Fluid Mechanics*, 2:417–445, 1957.
12. W. J. Pierson and L. Moskowitz. A proposed spectral form for fully developed wind seas based on similarity theory of S. A. Kilaigorodskii. *Journal of Geophysical Research*, 5181–5190, 1964.
13. K. T. Hasselman. Measurements of wind-wave growth swell decay during the Joint North Sea wave project (JONSWAP). *Erganzungsheft zur Deutch. Hydrogr. Zeit.*, 1973.
14. S. Haver. Analysis of uncertainties related to the stochastic modelling of ocean waves, *PhD Thesis*, The Norwegian Institute of Technology, July 1980.
15. I. R. Young. *Wind Generated Ocean Waves*. Elsevier, Amsterdam, 1999.
16. E. C. Monahan and G. MacNiocaill, editors. *Oceanic Whitecaps: Their Role in Air Sea Exchange Processes*. Dordrecht, Reidel, 1986.
17. P. Koepke. Effective reflectance of oceanic whitecaps. *Applied Optics*, 1816–1824, 1984.
18. C. Schlick. An inexpensive BRDF model for physically-based rendering. *Computer Graphics Forum*, 13(3):233–246, 1994.
19. N. G. Jerlov. *Marine Optics*. Elsevier, Amsterdam, 1976.
20. C. D. Mobley. *Light and Water. Radiative Transfer in Natural Waters*. Academic Press, New York, 1994.
21. R. W. Preisendorfer. *Hydrologic Optics*. National Technical Information Center, 1976.
22. R. W. Austin and T. J. Petzold. Spectral dependence of the diffuse attenuation coefficient of light in ocean water. *Optical Engineering*, 25(3):471–1986.
23. T. J. Petzold. *Light in the Sea*, Stroudsberg, pages 150–174. 1977.

24. H. R. Gordon. Can the Lambert–Beer law be applied to the diffuse attenuation coefficient of ocean water? *Limnol. Oceanogr.*, 34(8):1389–1989.

25. R. W. Gould Jr., R. A. Arnone and P. M. Martinolich. Spectral dependence of the scattering coefficient in case 1 and case 2 waters. *Applied Optics*, 38(12):2377–2383, 1999.

26. A. J. Preetham, P. Shirley and B. Smits. A practical analytic model for daylight. *Proceedings of SIGGRAPH 99*, 91–100, August 1999.

27. A. Morel. Optical modeling of the upper ocean in relation to its biogenus matter content (case I waters). *Journal of Geophysical Research*, 93(C9):10,749–10,768, 1988.

28. J. T. Kajiya. The rendering equation. In D. C. Evans and R. J. Athay (eds), *Computer Graphics (SIGGRAPH '86 Proceedings)*. volume 20, pages 143–150. August 1986.

29. S. Crone. `http://puffin.curtin.edu.au/~crones`.

30. M. P. Fairclough. `http://www.planetside.co.uk`. Terragen.

31. G. Spencer, P. Shirley, K. Zimmerman and D. Greenberg. Physically-based glare effects for digital images. In R. Cook (ed), *SIGGRAPH 95 Conference Proceedings*. Annual Conference Series, pages 325–334. ACM SIGGRAPH, Addison Wesley, August 1995, held in Los Angeles, California, 6–11. August 1995.